Optical properties of $TlNi_2Se_2$: Observation of pseudogap formation

X. B. Wang,[1] H. P. Wang,[1] Hangdong Wang,[2] Minghu Fang,[2,3] and N. L. Wang[4,5,*]

[1]*Beijing National Laboratory for Condensed Matter Physics, Institute of Physics, Chinese Academy of Sciences, Beijing 100190, China*

[2]*Department of Physics, Zhejiang University, Hangzhou 310027, China*

[3]*Collaborative Innovation Center of Advanced Microstructures, Nanjing 210093, China*

[4]*International Center for Quantum Materials, School of Physics, Peking University, Beijing 100871, China*

[5]*Collaborative Innovation Center of Quantum Matter, Beijing, China*

(Received 6 July 2015; published 23 December 2015)

The quasi-two-dimensional nickel chalcogenide $TlNi_2Se_2$ is a newly discovered superconductor. We have performed an optical spectroscopy study on $TlNi_2Se_2$ single crystals over a broad frequency range at various temperatures. The overall optical reflectance spectra are similar to those observed in its isostructure $BaNi_2As_2$. Both the suppression in $R(\omega)$ and the peaklike feature in $\sigma_1(\omega)$ suggest the progressive formation of a pseudogap feature in the mid-infrared range with decreasing temperatures, which might originate from the dynamic local fluctuation of the charge-density-wave (CDW) instability. We propose that the CDW instability in $TlNi_2Se_2$ is driven by the saddle-point mechanism, due to the existence of a van Hove singularity very close to the Fermi energy.

DOI: 10.1103/PhysRevB.92.245129 PACS number(s): 74.70.Xa, 74.70.−b, 74.25.Gz, 74.72.Kf

I. INTRODUCTION

The discovery of iron-based superconductors is the most significant breakthrough in condensed matter physics in recent years [1]. The iron-pnictides/chalcogenides are close to magnetism and it is widely believed that the spin fluctuation is responsible for the pairing of the superconducting electrons [2,3]. Compared with the iron-based compounds, the nickel-based systems have much lower critical temperature, for example, LaONiP ($T_c = 3$ K) [4], LaONiAs ($T_c = 2.7$ K) [5], $BaNi_2P_2$ ($T_c = 2.4$ K) [6], and $BaNi_2As_2$ ($T_c = 0.7$ K) [7], usually lower than 5 K even upon doping [5]. To date, no evidence for ordered or even fluctuated magnetism associated with Ni in proximity to superconductivity is found. Moreover, the majority of evidence suggests that the Ni-based systems can be understood in the context of conventional electron-phonon theory [8–11].

Recently, three nickel chalcogenides KNi_2Se_2 ($T_c \simeq 0.8$ K) [12], KNi_2S_2 ($T_c \simeq 0.46$ K) [13], and $TlNi_2Se_2$ ($T_c \simeq 3.7$ K) [14] were reported, in which superconductivity appears to involve heavy-fermion behavior below a coherent temperature $T_{coh} \sim 20$ K. In contrast to $K_xFe_{2-y}Se_2$ [15,16], the $TlNi_2Se_2$ compound is homogeneous without Ni vacancy or phase separation [12,14]. Considering the monovalent Tl or K in the stoichiometry composition, the effective valance of Ni in such compound is "1.5+". The mixed valency of $Ni^{1.5+}$ was proposed to induce the heavy effective band mass [12,13,17]. However, very recently, angle-resolved photoemission spectroscopy (ARPES) measurement [18] has revealed that $TlNi_2Se_2$ shares a universal band structure with $BaFe_2As_2$ [19] and $BaCo_2As_2$ [20], with a chemical potential shifted due to more $3d$ electrons in $TlNi_2Se_2$ ($3d^{8.5}$) than in $BaFe_2As_2$ ($3d^6$) and $BaCo_2As_2$ ($3d^7$). Therefore, it can be viewed as heavily electron doped $TlFe_2Se_2$ ($3d^{6.5}$), with reduced electronic correlations compared to its cousin $K_xFe_{2-y}Se_2$ [21]. Furthermore, the camelback-shaped band at the Z point gives rise to a pronounced van Hove singularity near Fermi energy (E_F), which provides a natural explanation to the heavy-electron behavior inferred from the electronic heat and the upper critical field measurements [14] in this weakly correlated system.

More specially, the neutron pair-distribution-function (PDF) analysis in a combined high-resolution synchrotron x-ray diffraction and neutron scattering study in KNi_2Se_2 reveals that the local charge-density-wave (CDW) state is present up to 300 K but disappears upon cooling in the "heavy-fermion" state below T_{coh} [12,13]. The effect is opposite to what is typically observed. Moreover the ARPES did not observe any anomaly in the spectra upon entering the fluctuating CDW state [22]. To understand the unique behavior, it is highly desirable to investigate the charge dynamics in the whole temperature range below 300 K.

Optical spectroscopy is a powerful bulk-sensitive technique with high-energy resolution, which is widely used to probe the carrier dynamics and possible gap formation of an electronic system. In this work, we present a detailed optical spectroscopy study of $TlNi_2Se_2$ single crystals. Our optical data reveal that $TlNi_2Se_2$ is a good metal with a distinct plasma reflectance edge, similar to its isostructure $BaNi_2As_2$. The overall frequency-dependent reflectivity $R(\omega)$ is gradually suppressed near 2500 cm^{-1} with decreasing temperature, and a pseudogap feature appears at any temperature below 300 K. The weak gap structure is attributed to the local CDW order or fluctuations. Our measurement indicates that the local CDW order/fluctuations are further enhanced at the lowest temperature, which is different from the neutron PDF analysis on KNi_2Se_2 in its "heavy-fermion state." In combination with the earlier ARPES results, we suggest that the fluctuating CDW instability is driven by the presence of saddle points in band structure which leads to the van Hove singularity close to the Fermi level.

II. EXPERIMENT

Single crystals of $TlNi_2Se_2$ were grown by the self-flux method [14]. Their structure, transport, magnetic, and thermodynamic properties have already been reported [14,23]. The frequency-dependent reflectance spectra at different

*nlwang@pku.edu.cn

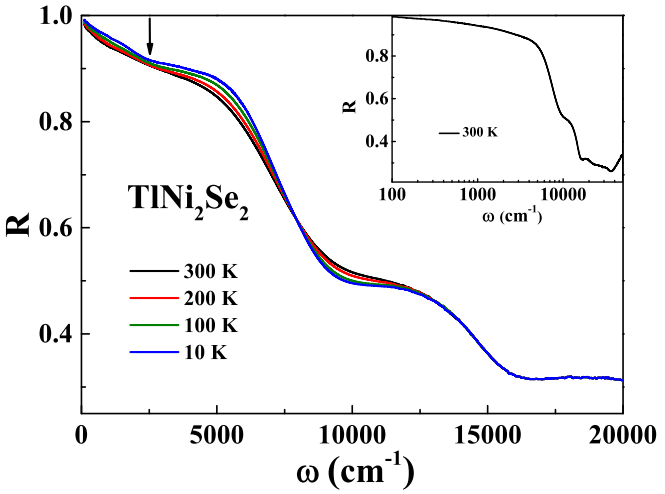

FIG. 1. (Color online) The temperature-dependent $R(\omega)$ in the frequency range from 100 to 20 000 cm^{-1}. The inset shows $R(\omega)$ data up to 50 000 cm^{-1} on a logarithmic scale at 300 K.

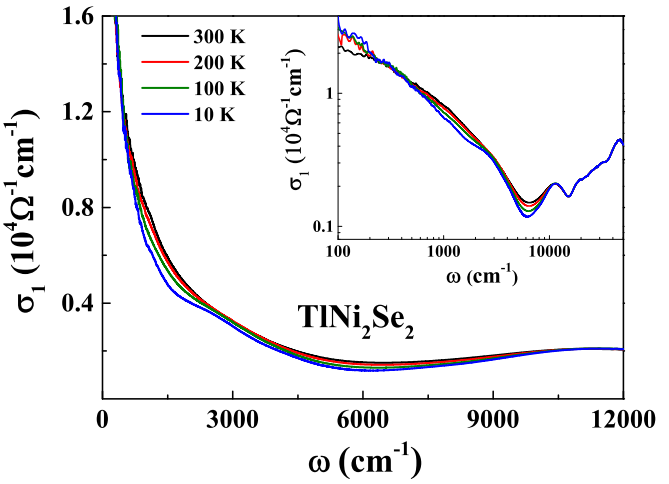

FIG. 2. (Color online) Frequency dependence of the optical conductivity below 12 000 cm^{-1} at different temperatures. The inset shows $\sigma_1(\omega)$ over broad frequencies up to 50 000 cm^{-1} on a logarithmic scale.

temperatures were measured by Bruker IFS 113v and 80v spectrometers in the frequency range from 30 to 20 000 cm^{-1} (4 meV $\sim$ 2.5 eV), and then the reflectance was extended to 50 000 cm^{-1} ($\sim$6.1 eV) at room temperature with a grating-type spectrometer. An *in situ* gold and aluminum overcoating technique was used to obtain the reflectivity $R(\omega)$. Considering the small size of our samples, the data below 100 cm^{-1} are cut off for reliability. The real part of conductivity $\sigma_1(\omega)$ is obtained by the Kramers-Kronig transformation of $R(\omega)$. The Hagen-Rubens relation was used for low-frequency extrapolation; on the high-frequency side, an extrapolation method using x-ray atomic scattering functions was applied to generate the high-frequency reflectivity [24].

III. RESULTS AND DISCUSSION

Figure 1 shows the reflectance spectra of $TlNi_2Se_2$ single crystals over a broad energy scale at various temperatures. The value of $R(\omega)$ approaches unity towards zero energy and shows an increase with decreasing temperature, indicating a good-metallic behavior. By lowering the temperature, we do not see any sharp changes in the optical spectra but rather weak suppression of $R(\omega)$ near 2500 cm^{-1}, signaling the opening of a partial gap (pseudogap). With increasing ω, $R(\omega)$ drops quickly near 7000 cm^{-1}, known as the screened plasma edge. The relativity high edge position reveals a high carrier density, which is similar to the isostructural compound $BaNi_2As_2$ [25]. There is another edge structure at about 15 000 cm^{-1} which is caused by an interband transition. The reflectivity becomes roughly temperature independent at higher frequencies. The inset of Fig. 1 shows $R(\omega)$ data up to 50 000 cm^{-1} in a logarithmic scale at 300 K.

Figure 2 shows the real part of conductivity spectra below 12 000 cm^{-1} at different temperatures. The Drude-type conductivity is observed for all spectra at low frequency and several temperature-independent interband transitions could be also well resolved, as shown in the inset of Fig. 2. The optical conductivity between 500 and 10 000 cm^{-1} is gradually suppressed and a broad peaklike feature becomes more and more obvious at 2800 cm^{-1} as the temperature decreases. The spectral line shape is similar to that of $BaFe_2As_2$ [26] across the spin-density-wave (SDW) transition though the feature is much weaker. It seems to suggest that there should also be a density-wave gap opening in $TlNi_2Se_2$. Furthermore, this pseudogap feature is most prominent at low temperature and can be resolved even in the 300 K data.

To quantify the temperature evolution of optical conductivity, especially the low-frequency components, we use a simple Drude-Lorentz model to decompose optical conductivity spectra [27]:

$$\sigma_1(\omega) = \sum_i \frac{\omega_{pi}^2}{4\pi} \frac{\Gamma_{Di}}{\omega^2 + \Gamma_{Di}^2} + \sum_j \frac{S_j^2}{4\pi} \frac{\Gamma_j \omega^2}{\left(\omega_j^2 - \omega^2\right)^2 + \omega^2 \Gamma_j^2}, \quad (1)$$

where ω_{pi} and Γ_{Di} are the plasma frequency and the relaxation rate of each conduction band, while ω_j, Γ_j, and S_j are the resonance frequency, the damping, and the mode strength of each Lorentz oscillator, respectively. This model includes Drude and Lorentz terms, which approximately capture the contribution by free carriers and interband transitions. Both transport [14,23] and ARPES [18] results suggest the multiband character of $TlNi_2Se_2$; therefore we applied two Drude components analysis here, similar to the other members of the "122" system [25–27]. Even though the Drude-Lorentz fit is somewhat arbitrary and the accuracy of the derived fit parameters is uncertain, it will not modify the key outcomes of the analysis.

Figure 3 illustrates the conductivity spectra at 300 K and 10 K together with the Drude-Lorentz fitting components at 10 K for $TlNi_2Se_2$. In order to reproduce the optical conductivity below 50 000 cm^{-1} at 300 K, two Drude components, a narrow and a broad one, and four Lorentz components have to be used. Furthermore, an additional mid-infrared peak is necessary near about 2800 cm^{-1} at any temperature below 300 K. We are mainly concerned about the evolution of the low-energy conductivity; therefore the fitting parameters for

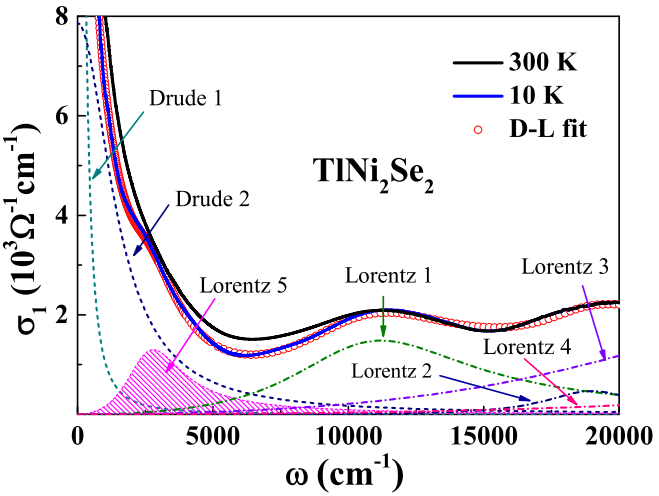

FIG. 3. (Color online) The experimental data of $\sigma_1(\omega)$ at 300 and 10 K with the Drude-Lorentz fits shown at the bottom.

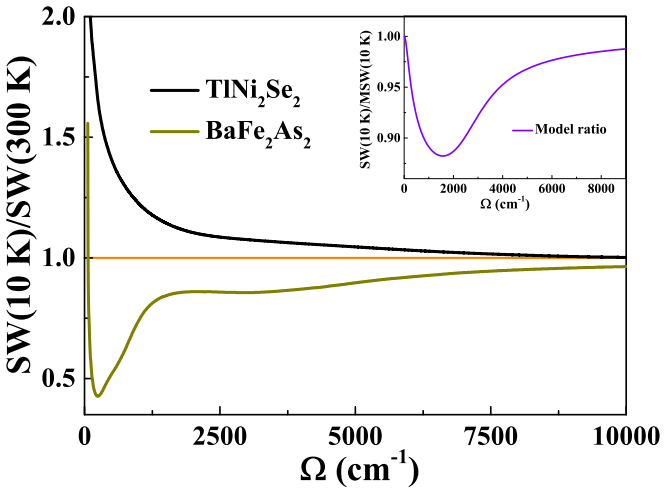

FIG. 4. (Color online) Ratio of the integrated spectral weight SW(10 K)/SW(300 K) as a function of cutoff frequency Ω in $TlNi_2Se_2$ and $BaFe_2As_2$. The inset shows the model ratio of the low-temperature integrated SW over that of the model optical conductivity at 10 K.

the the two Drude components are shown in Table I for different temperatures. We also show the error bars of the fitting parameters corresponding to an absolute error of 0.5% in reflectivity. We find that the two Drude components narrow with decreasing temperature due to the metallic response. The plasma frequency ω_{p1} keeps roughly unchanged, while ω_{p2} decreases suggesting that the gapping of the Fermi surfaces mainly appears in the broad Drude component. The Lorentz 5 oscillator strength S_5 increases continuously with decreasing temperature, indicating the progressive formation of the absorption peaks just above the pseudogap. We use the formula $\omega_p = \sqrt{\omega_{p1}^2 + \omega_{p2}^2}$ to estimate the overall plasma frequency; then we get $\omega_p \approx 36\,360\ \mathrm{cm}^{-1}$ at 300 K and 32 400 cm^{-1} at 10 K, respectively. Therefore, the ratio of the square of the plasma frequency at 10 K to that of 300 K is about 0.80. It is well known that $\omega_p^2 = 4\pi ne^2/m^*$, where n is the carrier density and m^* is the effective mass. If we assume that the effective mass of itinerant carriers would not change with temperature, the optical data reveal that roughly 20% of the itinerant carriers are lost due to the pseudogap opening at the Fermi surface.

TABLE I. The fitting parameters of two Drude components for $TlNi_2Se_2$ at different temperatures. ω_{p1} and ω_{p2} are the plasma frequencies of the narrow Drude term and the broad Drude term, respectively, Γ_{D1} and Γ_{D2} are the scattering ranges of the narrow Drude term and the broad Drude term, respectively. S_5 is the mode strength of the Lorentz 5 oscillator. The parameters of the model optical conductivity as discussed in the text are also given. The shown error bars correspond to an absolute error of 0.5% in reflectivity. The unit of these quantities is cm^{-1}.

T (K)	ω_{p1}	Γ_{D1}	ω_{p2}	Γ_{D2}	S_5	$\sqrt{\omega_{p1}^2+\omega_{p2}^2}$
300	18500	390	31300	2600	0	36360
200	18500	310	29400	2200	9500	34740
100	18500	270	27700	1900	12000	33310
10	18500	200	26600	1500	14100	32400
Model	18500	217	30100	1500	0	35300
Error bars	±300	±15	±400	±50	±300	

To further characterize the spectral evolution, we plot the integrated spectral weight of $TlNi_2Se_2$ at 10 K, as shown in Fig. 4, where the low-temperature integrated spectral weight has been normalized to the integrated spectral weight at room temperature. The optical spectral weight is defined as $\mathrm{SW} = \int_0^\Omega \sigma_1(\omega)d\omega$. For the convenience of comparison, we also present the low-temperature integrated spectral weight of $BaFe_2As_2$ [26]. For $BaFe_2As_2$, the strong dip below 1000 cm^{-1} represents the formation of the SDW gap in the magnetic ordered state [26], while the second dip near 3000 cm^{-1} reflects the unconventional SW transfer at high energy which seems to be a common feature in iron-pnictides/chalcogenides [28]. Nevertheless, for $TlNi_2Se_2$, the temperature-dependent spectral change is very different. The SW ratio exceeds 1 before it recovers to unity suggesting that the SW is transferred from high to low energy at low temperature. We should remark that most of the SW below 6000 cm^{-1} (the minimum of optical conductivity) would come from the intraband transitions. As the temperature decreases, the SW transformation from high to low energy is induced by the Drude components narrowing. This is the typical optical response of a metallic material. On the other hand, the pseudogap develops below 2000 cm^{-1} at low temperature. However, we note that the effects of the pseudogap formation to the SW transfer are minimal. It is the metallic response that leads to the SW transfer to low energy. In other words, the pseudogap is too weak to change the SW evolution in such a good metal. Notably, the SW of the mid-infrared peak could not fully compensate for the loss of the low-energy Drude component, and the recovery of the SW extends to a fairly high energy scale. Furthermore, the high-energy SW transfer above 8000 cm^{-1} is almost indistinguishable in $TlNi_2Se_2$. This may be related to the weaker correlation or Hund's coupling effect in $TlNi_2Se_2$ as compared to $BaFe_2As_2$, in agreement with the ARPES results [18,22].

In order to make the pseudogap-like suppression more clear, we also plot a model ratio of the low-temperature integrated SW to the model-integrated spectral weight at 10 K. Assuming that $TlNi_2Se_2$ is a pure metal without the pseudogap feature, the model optical conductivity at 10 K could be obtained according to the Drude-Lorentz model with two Drude components and four Lorentz components, as the situation at 300 K. The parameters of the model optical conductivity are listed in Table I, where Γ_{D1} is set to 217 cm^{-1} in order to keep the same dc optical conductivity as the real data and ω_{p2} is set to 30 100 cm^{-1} to conserve the total spectral weight at 10 K. We then normalize the integrated SW at low temperature SW(10 K) to the model value MSW(10 K). As shown in the inset of Fig. 4, the ratio decreases below $\approx$1700 cm^{-1}, suggesting that the SW is depleted due to opening of the pseudogap, and the suppressed SW is transferred to higher energy, leading to the gradual recovery of the SW above the pseudogap. This is a typical behavior of gap opening induced SW transformation.

Now we can summarize the main finding of our optical data: the overall optical spectra are similar to those observed in its isostructure $BaNi_2As_2$. Corresponding to the weak suppression of $R(\omega)$, the real part of the conductivity $\sigma_1(\omega)$ shows a suppression roughly below 2000 cm^{-1}, which leads to a peak above this energy. The mid-infrared peak is present at all measurement temperatures below 300 K, and becomes more and more obvious with decreasing temperature, indicating the gradual formation of the pseudogap. At the same time, irrespective of the uncertainly, the overall plasma frequency decreases, implying the partial gap opening on the Fermi surface, which gives further proof of the pseudogap formation. In particular, the SW transformation to higher energy induced by the pseudogap could be clearly observed in the model ratio, where we use the metallic response at 10 K as a reference.

As we have mentioned above, for KNi_2Se_2 or KNi_2S_2, the neutron PDF analysis suggested that the local CDW fluctuations are present at high temperature but disappear upon further cooling [12,13]. However, our optical data of $TlNi_2Se_2$ single crystals reveal the progressive formation of a pseudogap in the mid-infrared range, especially below T_{coh}. To understand the origin of the pseudogap in $TlNi_2Se_2$ crystals, there are also a few other experimental facts which should be taken into account. First, to date no evidence for magnetic transition was found in such nickel chalcogenides. Second, no static density wave, such as CDW or SDW, has been observed. Third, the anisotropy in $TlNi_2Se_2$ is rather small, although the compound has a layer structure. It appears that the pseudogap in $TlNi_2Se_2$ might originate from local CDW fluctuations, in agreement with earlier neutron measurement on KNi_2Se_2 and KNi_2S_2 [12,13]. Moreover, the local CDW fluctuation was suggested to be entirely dynamic and/or spatially incoherent [12,13], in contrast to the coherence CDWs observed in structurally related compounds such as *2H*-typed transition metal dichalcogenides [29]. With such CDW fluctuation, there could be a partial gap opening in k space on the Fermi surface, which could be related to the pseudogap feature in $TlNi_2Se_2$. However, different from KNi_2Se_2 and KNi_2S_2 where the fluctuated CDW order tends to disappear upon entering the heavy-electron state at very low temperature, the optical measurement on $TlNi_2Se_2$ indicates that the partial gap feature is further enhanced at the lowest temperature.

An earlier angle-resolved photoemission spectroscopy measurement on KNi_2Se_2 crystals suggested the quasi-two-dimensional nature of the Fermi surface and that the partially nested Fermi surface might be responsible for the local CDW fluctuations [22]. However, a more recent ARPES measurement on $TlNi_2Se_2$ revealed a more complicated and three-dimensional Fermi surface shape. Thus, a naive picture for a Fermi surface nesting scenario is not applicable here on $TlNi_2Se_2$. Furthermore, a camelback-shaped band near Fermi energy at the Z point was identified; in particular, the existence of four flat parts of the dispersion very close to E_F would give rise to a pronounced van Hove singularity [18]. On this basis, the CDW instability can be naturally understood in the framework of a "saddle-point" CDW mechanism, proposed by Rice and Scott [30]. The four saddle points near the Z point in $TlNi_2Se_2$ give a divergent contribution to the Lindhard response function $\chi(q)$, where q is a wave vector connecting two saddle points, leading to a CDW instability.

IV. SUMMARY

We have performed an optical spectroscopy study on $TlNi_2Se_2$ over a broad frequency range at various temperatures. Both the suppression in $R(\omega)$ and the peaklike feature in $\sigma_1(\omega)$ suggest the progressive formation of a pseudogap feature in the mid-infrared range with decreasing temperatures, which might originate from the dynamic local fluctuation of the charge-density-wave (CDW) instability. The CDW instability in $TlNi_2Se_2$ may not be driven by Fermi surface nesting, but by the saddle-point mechanism, due to the exitance of a van Hove singularity very close to the Fermi energy.

ACKNOWLEDGMENTS

This work is supported by the National Science Foundation of China (Grants No. 11120101003, 11327806, and 11374261), and by the 973 project of the Ministry of Science and Technology of China (Grant No. 2012CB821403).

[1] Y. Kamihara, T. Watanabe, M. Hirano, and H. Hosono, J. Am. Chem. Soc. **130**, 3296 (2008).
[2] I. I. Mazin, D. J. Singh, M. D. Johannes, and M. H. Du, Phys. Rev. Lett. **101**, 057003 (2008).
[3] A. Chubukov, Annu. Rev. Condens. Matter Phys. **3**, 57 (2012).
[4] T. Watanabe, H. Yanagi, T. Kamiya, Y. Kamihara, H. Hiramatsu, M. Hirano, and H. Hosono, Inorg. Chem. **46**, 7719 (2007).
[5] Z. Li, G. Chen, J. Dong, G. Li, W. Hu, D. Wu, S. Su, P. Zheng, T. Xiang, N. Wang, and J. Luo, Phys. Rev. B **78**, 060504 (2008).
[6] Y. Tomioka, S. Ishida, M. Nakajima, T. Ito, H. Kito, A. Iyo, H. Eisaki, and S. Uchida, Phys. Rev. B **79**, 132506 (2009).

[7] F. Ronning, N. Kurita, E. D. Bauer, B. L. Scott, T. Park, T. Klimczuk, R. Movshovich, and J. D. Thompson, J. Phys.: Condens. Matter **20**, 342203 (2008).
[8] Alaska Subedi and David J. Singh, Phys. Rev. B **78**, 132511 (2008).
[9] I. R. Shein and A. L. Ivanovskii, Phys. Rev. B **79**, 054510 (2009).
[10] B. Zhou, M. Xu, Y. Zhang, G. Xu, C. He, L. X. Yang, F. Chen, B. P. Xie, X. Y. Cui, M. Arita, K. Shimada, H. Namatame, M. Taniguchi, X. Dai, and D. L. Feng, Phys. Rev. B **83**, 035110 (2011).
[11] S. Ideta, T. Yoshida, M. Nakajima, W. Malaeb, H. Kito, H. Eisaki, A. Iyo, Y. Tomioka, T. Ito, K. Kihou, C. H. Lee, Y. Kotani, K. Ono, S. K. Mo, Z. Hussain, Z.-X. Shen, H. Harima, S. Uchida, and A. Fujimori, Phys. Rev. B **89**, 195138 (2014).
[12] J. R. Neilson, A. Llobet, A. V. Stier, L. Wu, J. Wen, J. Tao, Y. Zhu, Z. B. Tesanovic, N. P. Armitage, and T. M. McQueen, Phys. Rev. B **86**, 054512 (2012).
[13] J. R. Neilson, T. M. McQueen, A. Llobet, J. Wen, and M. R. Suchomel, Phys. Rev. B **87**, 045124 (2013).
[14] H. Wang, C. Dong, Q. Mao, R. Khan, X. Zhou, C. Li, B. Chen, J. Yang, Q. Su, and M. Fang, Phys. Rev. Lett. **111**, 207001 (2013).
[15] W. Li, H. Ding, P. Deng, K. Chang, C. Song, K. He, L. Wang, X. Ma, J.-P. Hu, X. Chen, and Q.-K. Xue, Nat. Phys. **8**, 126 (2012).
[16] Z. Wang, Y. J. Song, H. L. Shi, Z. W. Wang, Z. Chen, H. F. Tian, G. F. Chen, J. G. Guo, H. X. Yang, and J. Q. Li, Phys. Rev. B **83**, 140505(R) (2011).
[17] James M. Murray and Zlatko Tesanovic, Phys. Rev. B **87**, 081103(R) (2013).
[18] N. Xu, C. E. Matt, P. Richard, A. van Roekeghem, S. Biermann, X. Shi, S.-F. Wu, H. W. Liu, D. Chen, T. Qian, N. C. Plumb, M. Radovic, H. Wang, Q. Mao, J. Du, M. Fang, J. Mesot, H. Ding, and M. Shi, Phys. Rev. B **92**, 081116 (2015).
[19] P. Richard, K. Nakayama, T. Sato, M. Neupane, Y.-M. Xu, J. H. Bowen, G. F. Chen, J. L. Luo, N. L. Wang, X. Dai, Z. Fang, H. Ding, and T. Takahashi, Phys. Rev. Lett. **104**, 137001 (2010).
[20] N. Xu, P. Richard, A. van Roekeghem, P. Zhang, H. Miao, W.-L. Zhang, T. Qian, M. Ferrero, A. S. Sefat, S. Biermann, and H. Ding, Phys. Rev. X **3**, 011006 (2013).
[21] T. Qian, X.-P. Wang, W.-C. Jin, P. Zhang, P. Richard, G. Xu, X. Dai, Z. Fang, J.-G. Guo, X.-L. Chen, and H. Ding, Phys. Rev. Lett. **106**, 187001 (2011).
[22] Q. Fan, X. P. Shen, M. Y. Li, D. W. Shen, W. Li, X. M. Xie, Q. Q. Ge, Z. R. Ye, S. Y. Tan, X. H. Niu, B. P. Xie, and D. L. Feng, Phys. Rev. B **91**, 125113 (2015).
[23] X. C. Hong, Z. Zhang, S. Y. Zhou, J. Pan, Y. Xu, H. Wang, Q. Mao, M. Fang, J. K. Dong, and S. Y. Li, Phys. Rev. B **90**, 060504 (2014).
[24] D. B. Tanner, Phys. Rev. B **91**, 035123 (2015).
[25] Z. G. Chen, G. Xu, W. Z. Hu, X. D. Zhang, P. Zheng, G. F. Chen, J. L. Luo, Z. Fang, and N. L. Wang, Phys. Rev. B **80**, 094506 (2009).
[26] W. Z. Hu, J. Dong, G. Li, Z. Li, P. Zheng, G. F. Chen, J. L. Luo, and N. L. Wang, Phys. Rev. Lett. **101**, 257005 (2008).
[27] D. Wu, N. Barisic, P. Kallina, A. Faridian, B. Gorshunov, N. Drichko, L. J. Li, X. Lin, G. H. Cao, Z. A. Xu, N. L. Wang, and M. Dressel, Phys. Rev. B **81**, 100512(R) (2010).
[28] N. L. Wang, W. Z. Hu, Z. G. Chen, R. H. Yuan, G. Li, G. F. Chen, and T. Xiang, J. Phys.: Condens. Matter **24**, 294202 (2012).
[29] W. Z. Hu, G. Li, J. Yan, H. H. Wen, G. Wu, X. H. Chen, and N. L. Wang, Phys. Rev. B **76**, 045103 (2007).
[30] T. M. Rice and G. K. Scott, Phys. Rev. Lett. **35**, 120 (1975).